AAC Journals.ASM.org

Dronedarone, an Amiodarone Analog with Improved Anti-*Leishmania mexicana* Efficacy

Gustavo Benaim,[a,b] Paola Casanova,[a,b] Vanessa Hernandez-Rodriguez,[a] Sheira Mujica-Gonzalez,[a] Nereida Parra-Gimenez,[a] Lourdes Plaza-Rojas,[a] Juan Luis Concepcion,[c] Yi-Liang Liu,[d] Eric Oldfield,[d,e] Alberto Paniz-Mondolfi,[f] Alirica I. Suarez[g]

Laboratorio de Señalización Celular y Bioquímica de Parasitos, Instituto de Estudios Avanzados (IDEA), Caracas, Venezuela[a]; Instituto de Biología Experimental, Facultad de Ciencias, Universidad Central de Venezuela (UCV), Caracas, Venezuela[b]; Laborartorio de Enzimologia de Parásitos, Facultad de Ciencias, Universidad de Los Andes, Mérida, Venezuela[c]; Center for Biophysics and Computational Biology, University of Illinois at Urbana-Champaign, Urbana, Illinois, USA[d]; Department of Chemistry, University of Illinois at Urbana-Champaign, Urbana, Illinois, USA[e]; Instituto de Biomedicina (MPPSPS/UCV)/Instituto Venezolano de los Seguros Sociales (IVSS), Caracas, Venezuela[f]; Facultad de Farmacia, Universidad Central de Venezuela, Caracas, Venezuela[g]

Dronedarone and amiodarone are cationic lipophilic benzofurans used to treat cardiac arrhythmias. They also have activity against the parasitic protozoan *Trypanosoma cruzi*, the causative agent of Chagas' disease. They function by disrupting intracellular Ca^{2+} homeostasis of the parasite and by inhibiting membrane sterol (ergosterol) biosynthesis. Amiodarone also has activity against *Leishmania mexicana*, suggesting that dronedarone might likewise be active against this organism. This might be of therapeutic interest, since dronedarone is thought to have fewer side effects in humans than does amiodarone. We show here that dronedarone effectively inhibits the growth of *L. mexicana* promastigotes in culture and, more importantly, has excellent activity against amastigotes inside infected macrophages (the clinically relevant form) without affecting the host cell, with the 50% inhibitory concentrations against amastigotes being 3 orders of magnitude lower than those obtained previously with *T. cruzi* amastigotes (0.65 nM versus 0.75 μM). As with amiodarone, dronedarone affects intracellular Ca^{2+} homeostasis in the parasite, inducing an elevation of intracellular Ca^{2+} levels. This is achieved by rapidly collapsing the mitochondrial membrane potential and inducing an alkalinization of acidocalcisomes at a rate that is faster than that observed with amiodarone. We also show that dronedarone inhibits parasite oxidosqualene cyclase, a key enzyme in ergosterol biosynthesis known to be vital for survival. Overall, our results suggest the possibility of repurposing dronedarone as a treatment for cutaneous, and perhaps other, leishmaniases.

Leishmania mexicana is a trypanosomatid parasite responsible for cutaneous and mucocutaneous leishmaniases. Drugs used to treat these diseases, such as meglumine antimoniate (Glucantime), amphotericin B, and miltefosine, frequently cause adverse side effects (1, 2) so there is a growing interest in new drug targets and leads. We have demonstrated that amiodarone (Fig. 1, compound 1), a commonly used antiarrhythmic, has promising activity against both *Leishmania mexicana* (3) and *Trypanosoma cruzi* parasites (4, 5). Moreover, the combination of amiodarone and miltefosine resulted in the complete parasitological cure of mice infected with *L. mexicana* (6). It has been proposed that disruption of parasite intracellular Ca^{2+} homeostasis is the target of action of several drugs, including miltefosine and amiodarone (7). Thus, miltefosine opens a Ca^{2+} channel in the plasma membrane of these parasites (6), probably related to the recently described sphingosine-induced L-type voltage-dependent Ca^{2+} channel in *L. mexicana* (8), causing a large increase in the intracellular Ca^{2+} concentration ($[Ca^{2+}]_i$) of the parasites, while amiodarone also increases the $[Ca^{2+}]_i$ in *L. mexicana* promastigotes, by collapsing the mitochondrial electrochemical potential and alkalinizing acidocalcisomes. However, in spite of its frequent use in humans, amiodarone use may lead to a number of side effects, due at least in part to the presence of two iodine atoms in its structure, which may contribute, for example, to its thyroid toxicity. For this reason, an analog of amiodarone that does not contain iodine (dronedarone) was developed (Fig. 1, compound 2). Recently, we found that dronedarone shows even greater potency than does amiodarone against *T. cruzi* epimastigotes and against amastigotes present in infected Vero cells, which constitute the clinically relevant form of the parasite (9). This opens the possibility of using dronedarone, already FDA approved for treating arrhythmias, against Chagas' disease (4) and, perhaps, leishmaniasis. Here, we report the effects of dronedarone on *L. mexicana*, finding that it has potent activity against both promastigotes and amastigotes inside macrophages, whose growth is not affected by the drug. As with amiodarone, dronedarone functions by disrupting Ca^{2+} homeostasis and by inhibiting parasite oxidosqualene cyclase (OSC), a key enzyme in ergosterol synthesis. This multisite targeting is likely to contribute to the potent activity found.

MATERIALS AND METHODS

Chemicals. Amiodarone (Fig. 1, compound 1), digitonin, EGTA, carbonyl cyanide *p*-(trifluoromethoxy)phenylhydrazone (FCCP), and nigericin were purchased from Sigma (St. Louis, MO). Fura 2-acetoxymethyl ester (fura 2-AM), acridine orange, rhodamine 123, and rhod 2-AM were from Molecular Probes (Eugene, OR).

Dronedarone extraction. At room temperature, two commercial tablets of dronedarone (Multaq, 400 mg each; Sanofi-Aventis) were added to 20 ml of methanol. Then 10 ml of H_2O was added, and the mixture was stirred for 15 min. The mixture was extracted with 10 ml of chloroform

Received 11 June 2013 Returned for modification 9 July 2013
Accepted 29 January 2014
Published ahead of print 3 February 2014
Address correspondence to Gustavo Benaim, gbenaim@idea.gob.ve.

doi:10.1128/AAC.01240-13

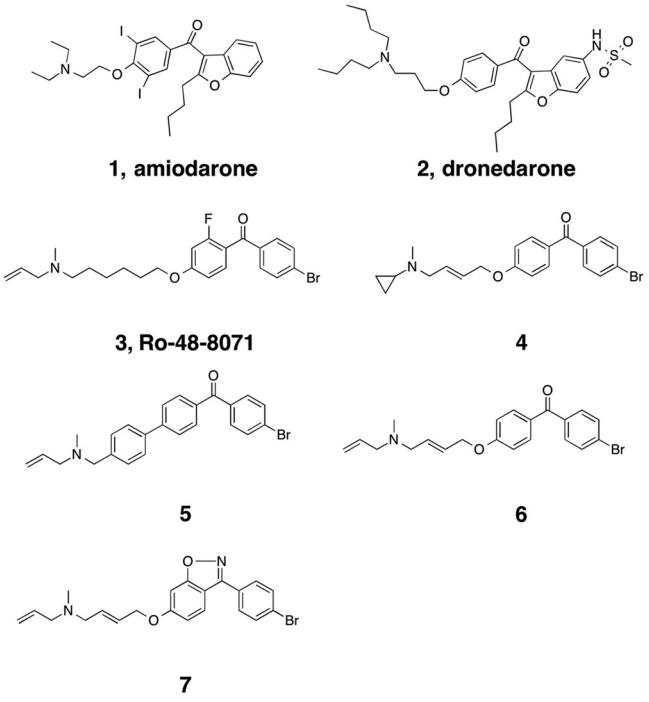

FIG 1 Structures of molecules of interest.

four times, and the combined chloroform extracts were dried over anhydrous magnesium sulfate, filtered, and evaporated under reduced pressure to yield colorless crystals. The product was further purified using column chromatography on silica gel (eluent chloroform-hexane, 9:1), and the fractions containing pure dronedarone were evaporated to obtain pure dronedarone as colorless crystals (mp 65°C).

Culture of *L. mexicana* epimastigotes and growth inhibition by dronedarone. *L. mexicana* (Bel 21 strain) promastigotes were cultured in liver infusion-tryptose (LIT) medium supplemented with 10% fetal bovine serum using continuous agitation (100 rpm) at 29°C, as reported previously (8). A growth curve was performed to evaluate the susceptibility of parasites to either dronedarone or amiodarone at different concentrations; live parasites were counted daily using a Neubauer chamber. The initial parasite concentration was 10^6 parasites/ml, and either the drug or the vehicle (dimethyl sulfoxide [DMSO]) was added after 24 h. At least 3 independent experiments were performed for each drug and dose, and the 50% inhibitory concentrations (IC_{50}s) were determined using GraphPad Prism 5.0.

Amastigote growth inhibition. *L. mexicana* amastigotes were incubated with murine macrophages (J774) maintained in RPMI 1640 (Gibco) supplemented with 10% fetal bovine serum at 37°C in humidified 95% air-5% CO_2 (6). Five hundred macrophages were seeded per coverslip in a 24-well plate and infected with promastigotes, using 10 parasites per cell, for 12 h. After infection, cells were washed three times to remove the external, nonadherent parasites, and fresh culture medium was added, with or without dronedarone at different concentrations. The infected cells were incubated for 96 h as previously described (6). After 96 h, macrophages were fixed with methanol and stained with Giemsa to determine the percentage of infected cells.

Determination of the intracellular Ca^{2+} concentration. *L. mexicana* promastigotes were loaded with the fluorescent ratiometric indicator fura 2 in order to evaluate the effect of dronedarone on $[Ca^{2+}]_i$ as reported previously (8). Briefly, 1×10^8 parasites were collected by centrifugation at $600 \times g$ for 2 min and washed twice with a loading buffer (137 mM NaCl, 4 mM KCl, 1.5 mM KH_2PO_4, 8.5 mM Na_2HPO_4, 11 mM glucose, 1 mM $CaCl_2$, 0.8 mM $MgSO_4$, and 20 mM HEPES-NaOH [pH 7.4]). The pellet was then resuspended and loaded with fura 2-AM (1 μM), probenecid (2.4 mM), and pluronic acid (0.05%) in the loading buffer. The parasites were incubated at 29°C in the dark with continuous agitation for 1 h. Fura 2-loaded parasites were washed twice with the same buffer, in either the presence or absence of Ca^{2+}. Fluorescence measurements were carried out on stirred cells at 29°C using a PerkinElmer LS 55 spectrofluorimeter with excitation (Ex) at 340 nm and 380 nm and emission (Em) at 510 nm.

The $[Ca^{2+}]_i$ was calculated as described by Grynkiewicz et al. (10), using the equation, $[Ca^{2+}]_i = K_d \times (R - R_{min}/R_{max} - R) \times F_{min}$ (380)/F_{max} (380), where K_d is the dissociation constant (244 nM), R is the ratio of measured fluorescence intensities (at 340 nm and at 380 nm), R_{min} is the lowest R value at 0 Ca^{2+} concentration, R_{max} is the highest R value at saturating concentrations of Ca^{2+}, F_{max} is the lowest value of measured fluorescence at 380 nm with 0 Ca^{2+} concentration, and F_{min} is the highest value of measured fluorescence at 380 nm at saturating concentrations of Ca^{2+}.

Maximum and minimum values were obtained after the addition of 30 μM digitonin, which allows the flow of Ca^{2+} to the interior of the cell. Then, 8 mM EGTA was added to chelate the remaining Ca^{2+}.

Mitochondrial membrane potential. The effect of dronedarone on the mitochondrial membrane potential of *L. mexicana* promastigotes was evaluated using the fluorescent dye rhodamine 123 as reported previously (9). Briefly, 10^8 parasites were collected by centrifugation at $600 \times g$ for 2 min and washed in phosphate-buffered saline (PBS) plus 1% glucose. The pellet was resuspended in the same buffer and loaded with 20 μM rhodamine 123 for 45 min at 29°C in the dark with mild agitation. Subsequently, parasites were washed twice, resuspended in the same buffer, and transferred into a magnetically stirred cuvette. Measurements (excitation wavelength [λ_{ext}], 488 nm; emission wavelength [λ_{em}], 530 nm) were made in a Hitachi 7000 spectrofluorimeter at 29°C. FCCP (1 μM) was used as a positive control.

Acidocalcisome alkalinization. The effect of dronedarone on the alkalinization of acidocalcisomes was evaluated using acridine orange (9). Promastigotes (10^8 cells/ml) were collected and washed and then incubated with 2 μM acridine orange in PBS for 5 min at 29°C with constant stirring. Measurements were performed with λ_{ext} at 488 nm and λ_{em} at 530 nm at 29°C in a Hitachi 7000 spectrofluorimeter under magnetic stirring. Nigericin (1 μM) was used as a positive control.

Subcellular fractionation. *L. mexicana* promastigotes in the exponential phase (2 liters of culture) were homogenized and fractionated following established procedures (11). Briefly, cells were collected at $3{,}000 \times g$ for 10 min and washed twice in buffer A (25 mM Tris-HCl [pH 7.4], 1 mM EDTA, 250 mM sucrose) and broken by abrasion in a 1:1 (wet weight/wt) mixture of cells with silicon carbide (200 mesh) in a chilled mortar to produce a homogenate that was diluted to 100 ml of buffer B (25 mM Tris-HCl [pH 7.2], 250 mM sucrose, 25 mM NaCl, 2 mM Na_2EDTA, 5 mM dithiothreitol) in the presence of a cocktail of protease inhibitors (10 μM leupeptin, 50 μg ml^{-1} trypsin inhibitor, 1 mM benzamidine, 50 μM phenylmethylsulfonyl fluoride (PMSF), 100 μM *N*α-*p*-tosyl-L-lysine chloromethyl ketone [TLCK], 0.2 μM antipain, 1 μM pepstatin, 1 μM E-64, 1 μM chymostatin, 1 μM bestatin). The homogenate was centrifuged at $1{,}000 \times g$ for 10 min to remove unbroken cells and nuclei and then at $5{,}000 \times g$ for 10 min, which produced a large granule fraction (containing mitochondria and large cellular debris); a small granule pellet was obtained at $33{,}000 \times g$ for 15 min. The post-small granule supernatant was subjected to $105{,}000 \times g$ for 90 min to produce a microsomal pellet and a soluble (cytosolic) fraction. The microsomal fraction pellet was resuspended in 6 ml of 50 mM morpholinepropanesulfonic acid (MOPS)-NaOH (pH 7.4), 1 mM EDTA, 0.1% Triton X-100, and 0.1% Tween 80, homogenized with a Potter-Elvehjem homogenizer, and then centrifuged at $105{,}000 \times g$ for 90 min. The resulting supernatant was collected and used for the enzyme inhibition assays.

Determination of protein concentration. Proteins were precipitated with 10% (wt/vol) trichloroacetic acid at 47°C. The protein precipitate

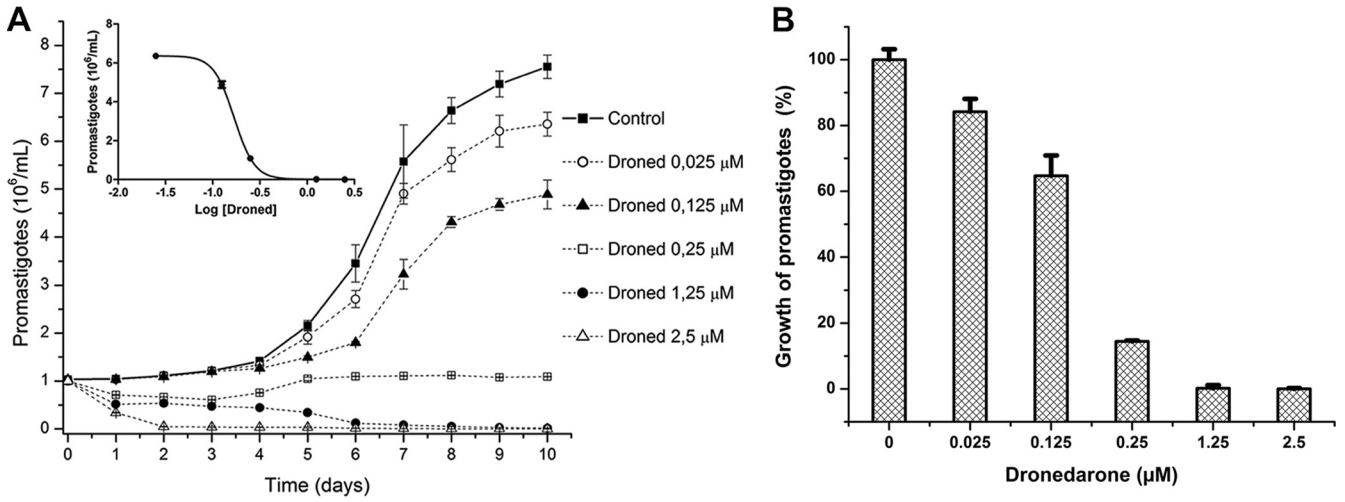

FIG 2 Inhibition of *L. mexicana* promastigotes growth by dronedarone. (A) Susceptibility of promastigotes to dronedarone (Droned). Each point represents the mean ± SD of at least three independent experiments. (Inset) Dose-response curve from panel A (IC_{50}, 115 nM). (B) Percentages of growth inhibition induced by dronedarone in promastigotes. All of the values were taken from the data of panel A, using the values obtained at 10 days after addition of the corresponding drug concentration. Each point represents the mean ± SD.

was washed with cold acetone, resuspended in distilled water, and finally assayed using a modification (12) of Folin phenol in the presence of 0.1% sodium dodecyl sulfate; the procedure was designed to eliminate the interference from substances present in the fractionation and assay media, including EDTA and sucrose. Bovine serum albumin was used as a standard.

Enzyme inhibition assay. Oxidosqualene cyclase (OSC) was assayed using the radioactive method described by Milla et al. (13). The microsomal extract (0.7 mg of protein/ml) was incubated with 3*S*-2,3-[^{14}C]oxidosqualene (35 μM) in the presence of Triton X-100 (0.1%) and Tween 80 (0.1%) in 50 mM MOPS-NaOH (pH 7.4) and 1 mM EDTA for 30 min at 28°C under vigorous shaking on a water bath. The reaction was stopped by addition of 20% KOH-50% ethanol (EtOH), and lipid was saponified at 80°C for 30 min. The nonsaponifiable lipids were extracted twice with 1 ml of petroleum ether and separated on thin-layer chromatography (TLC) plates (Merck) using toluene-diethyl ether (9:1) as the developing solvent. Radioactivity in 2,3-oxidosqualene and lanosterol was quantified by using an imaging plate on a System 2000 imaging scanner (Packard). The amount of lanosterol product formed was used for the calculation of enzyme activity. Chromatographic standards were 2,3,22,23-dioxidosqualene, lanosterol, squalene, 2,3-oxidosqualene, and ergosterol. The standards were visualized on the TLC plate with iodine vapor. The enzyme inhibition was carried out in basically the same way, but in the presence of various concentrations of dronedarone. Lineweaver-Burk plots were utilized to derive apparent K_i values (averages of triplicates ± standard deviation [SD]).

Computational aspect. Docking of dronedarone to a Phyre2 (14) model of *L. mexicana* OSC (LmOSC) was carried out by using the Glide program (15) from Schrödinger. The common feature hypothesis was produced using compounds 3 to 7, known OSC inhibitors (5), with the Molecular Operating Environment (MOE) program (16). All the structural figures were made by using PyMOL (17).

Data analysis. Kinetic data and IC_{50} results were analyzed using nonlinear regression methods implemented in the SigmaPlot software package.

RESULTS AND DISCUSSION

We first studied the effect of dronedarone at different concentrations on the growth of *L. mexicana* promastigotes. Figure 2A shows that dronedarone at concentrations of >0.25 μM has a profound effect on the growth of promastigotes in culture. The calculated IC_{50} was 115 nM (as shown in the inset). This concentration is much smaller than the concentration that we previously obtained in *L. mexicana* with amiodarone (IC_{50} of ~900 nM) (6). We also analyzed the percentage of growth inhibition induced by dronedarone in promastigotes in Fig. 2B, where a clear dose-dependent response was obtained. We then evaluated the effect of dronedarone on the growth of intracellular amastigotes in the infected macrophages. As shown in Fig. 3, dronedarone has a marked effect on the parasites, with a calculated IC_{50} of 0.65 nM, again significantly less than the IC_{50} of 8 nM observed using amiodarone under the same conditions (6). Interestingly, this concentration is also dramatically lower than that obtained using

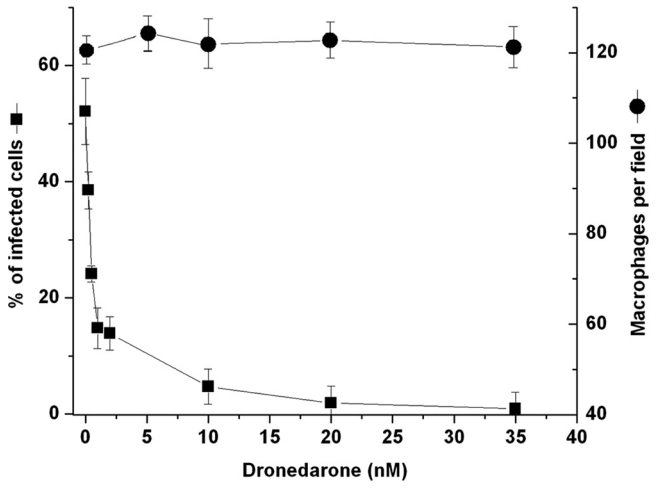

FIG 3 Effect of dronedarone against intracellular amastigotes. Macrophages (J774 cells) infected with *L. mexicana* amastigotes were exposed to different concentrations of dronedarone. The percentages of infected macrophages and the effects on noninfected macrophages were determined at 72 h after the addition of the drug. Around 100 cells were counted in each experiment. Each point represents the mean ± SD of at least three independent experiments.

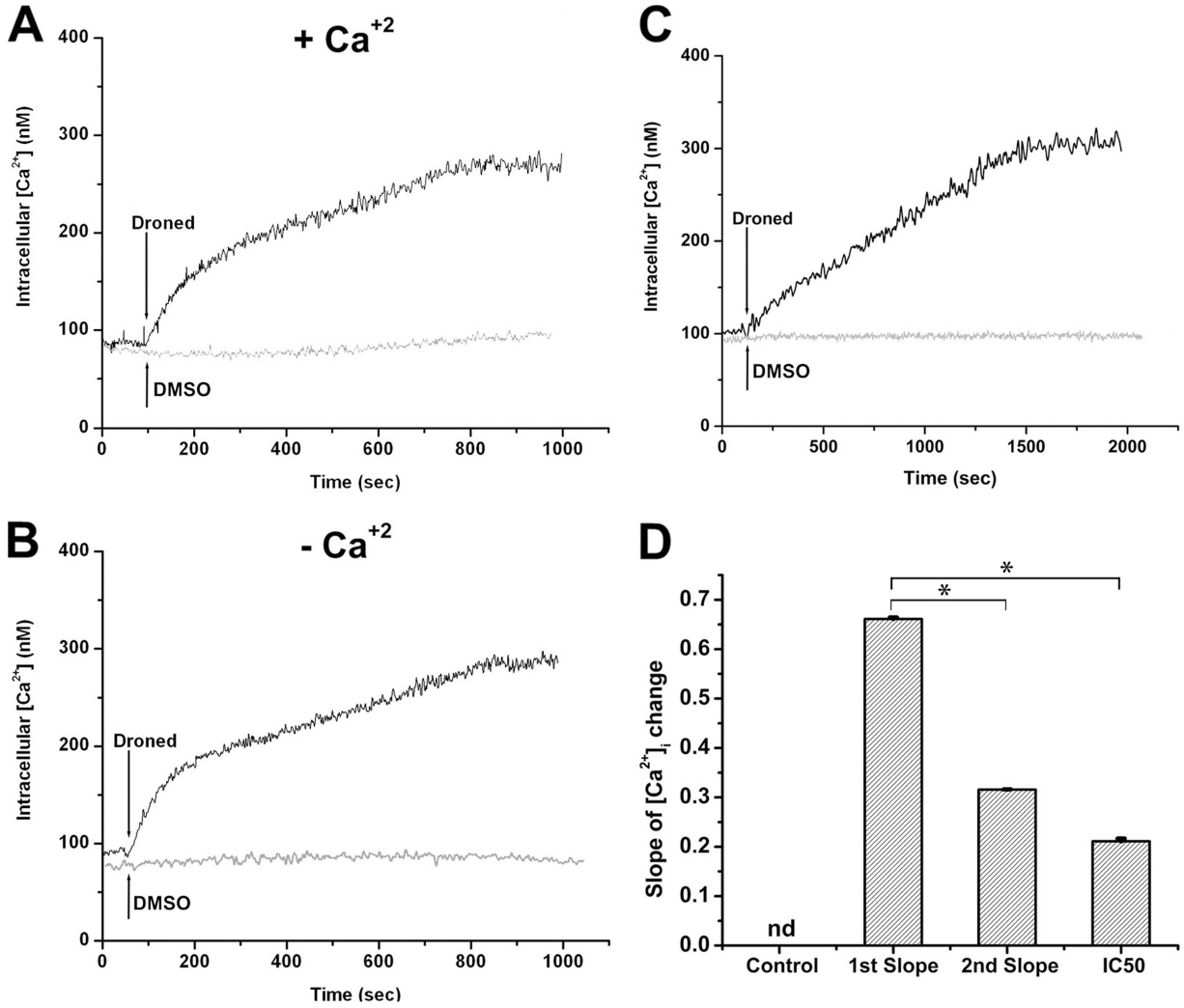

FIG 4 Effect of dronedarone (Droned) on the $[Ca^{2+}]_i$ of *L. mexicana* promastigotes. Promastigotes were loaded as described under Materials and Methods. (A) Effect of 2.5 μM dronedarone (arrow) on the parasite cytoplasmic Ca^{2+} concentration in the presence of 2 mM external Ca^{2+}. (B) Effect of 2.5 μM dronedarone (arrow) on fura 2-loaded promastigotes in the absence of external Ca^{2+} (EGTA). (C) Effect of 0.65 nM dronedarone (arrow) on the parasite cytoplasmic Ca^{2+} concentration in the presence of 2 mM external Ca^{2+}. The figures shown are representative of at least three independent experiments. (D) Initial slopes (300 s) of the curves obtained in the presence of 2 mM external Ca^{2+}. The first and second slopes were taken from at least three independent experiments similar to that shown in panel A. The slope named IC_{50} was taken from at least three independent experiments similar to that shown in panel C. Each point represents the mean ± SD. *, significant difference (measured using Student's *t* test, $P < 0.01$); nd, not determined.

dronedarone on *T. cruzi* amastigotes in infected cells, for which in a previous work (9) we reported an IC_{50} of 0.75 μM (i.e., an ~1,000-fold-higher IC_{50}). Since the amastigotes inside macrophages represent the clinically relevant form of *L. mexicana*, this result points to the much higher effectiveness of dronedarone in *L. mexicana*. Additionally, it can be seen (Fig. 3) that dronedarone at the concentrations employed does not have any discernible effect on macrophages over the entire dose range investigated. At therapeutic doses (in humans to treat arrhythmias), the plasma level of dronedarone is ~0.2 μM, but in the liver, the level is ~10 to 20 times higher (18).

The 0.65 nM IC_{50} in amastigotes is ~300 times less than the 0.2 μM plasma level using normal therapeutic dosing and suggests a potentially good therapeutic index.

Since we found in previous work that amiodarone induced an increase in the intracellular cytoplasmic levels of calcium ($[Ca^{2+}]_i$), we next investigated whether dronedarone had a similar effect on $[Ca^{2+}]_i$ using fura 2-loaded promastigotes. As shown in Fig. 4A, the addition of dronedarone (2.5 μM) induces a marked increase in $[Ca^{2+}]_i$, which reaches a plateau after a few minutes. To determine whether this increase was due to entry of extracellular Ca^{2+} or was a consequence of its release from intracellular organelles, the same experiment was performed in the absence of external Ca^{2+} (i.e., a Ca^{2+}-free buffer and the presence of EGTA). As can be seen in Fig. 4B, in the absence of external calcium, dronedarone causes the same increase in $[Ca^{2+}]_i$ as that obtained in the presence of external calcium, meaning that it was released from intracellular stores. It should be noticed that under both conditions, we observed a biphasic response that we attribute to the action of dronedarone on at least two intracellular compartments, namely, acidocalcisomes and the mitochondrion, given that these are the intracellular organelles known to be involved in

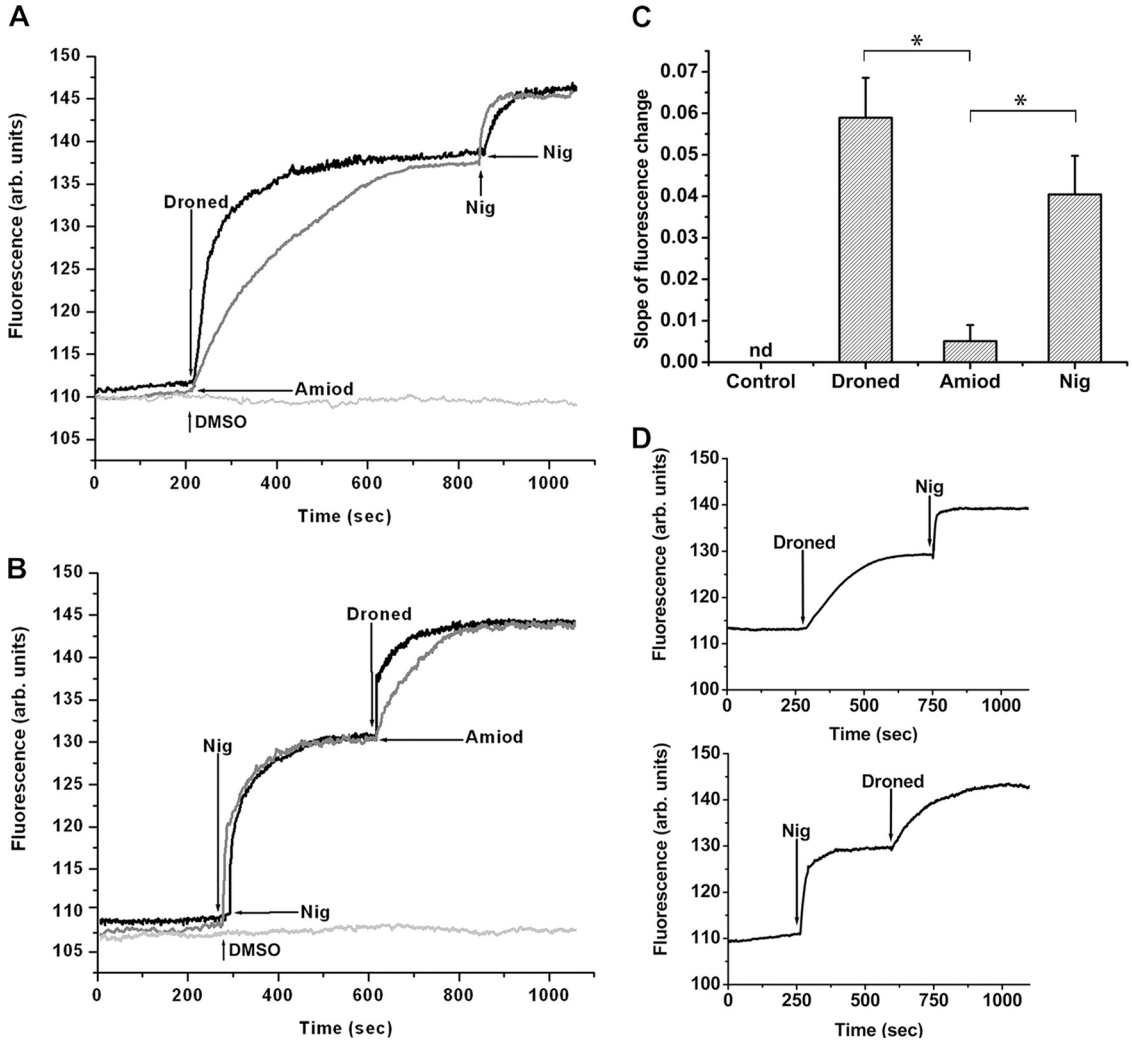

FIG 5 Effect of dronedarone on acidocalcisomes from *L. mexicana* promastigotes. Parasites were loaded with acridine orange (2 μM) as described in Materials and Methods. The excitation wavelength was 488 nm, and the emission wavelength was 530 nm. (A) Upper black trace, effect of dronedarone (Droned, 2.5 μM), followed by the addition of nigericin (Nig, 2 μM) on the acidic level of acidocalcisomes. Lower gray trace, effect of amiodarone (Amiod, 10 μM) and then of nigericin (2 μM) on the acidic level of acidocalcisomes. The additions in panel B are in reverse order versus those in panel A. (C) Initial slopes (250 s) of the curves from experiments similar to that of panels A and B. The slopes corresponding to dronedarone and amiodarone were taken from at least three independent experiments similar to that shown in panel A. The slope corresponding to nigericin was taken from at least three independent experiments similar to that shown in panel B. Each point represents the mean ± SD. *, significant difference (measured using Student's *t* test, $P < 0.01$). (D) Top, effect of dronedarone (6.5 nM) followed by the addition of nigericin (2 μM) on the acidic level of acidocalcisomes; bottom, effects of nigericin (2 μM) and then dronedarone (6.5 nM) on the acidic level of acidocalcisomes. The figures shown are representative of at least three independent experiments.

Ca^{2+} accumulation (7, 19, 20). We calculated the initial slopes of this biphasic response, finding that dronedarone acts about twice as fast as does amiodarone (Fig. 4D). However, when the experiments were performed using the IC_{50} instead of 2.5 μM dronedarone (Fig. 4C), there was still a marked increase in $[Ca^{2+}]_i$, but the biphasic response was not discernible and the initial slope of the curve with dronedarone was about one-third of that obtained in the presence of the drug at 2.5 μM (Fig. 4D).

In order to test the effect of dronedarone on acidocalcisomes, several experiments were performed using promastigotes loaded with acridine orange, a compound that accumulates in acidic compartments, enabling the visualization of any alkalinization. Figure 4A shows that dronedarone (2.5 μM) induces rapid alkalinization of acidocalcisomes. In the same experiment, amiodarone, also known to lower the acidity in these organelles (6), was added at 10 μM in order to compare its effect with that of dronedarone. As can be seen in Fig. 5A, the effect of dronedarone was significantly faster than that seen with amiodarone. The subsequent addition of nigericin induced further alkalinization in these organelles (Fig. 5A). Nigericin promotes the electroneutral exchange of H^+ and K^+, and loading with acridine orange followed by exposure to nigericin leads to the rapid release of the fluorescent dye from the acidocalcisomes with a concomitant increase in fluorescence (9).

Performing the same experiment but inverting the order of addition (i.e., adding nigericin first and then dronedarone or amiodarone) produced once again a large rise in acidocalcisome alkalinization (Fig. 5B). The subsequent addition of dronedarone or

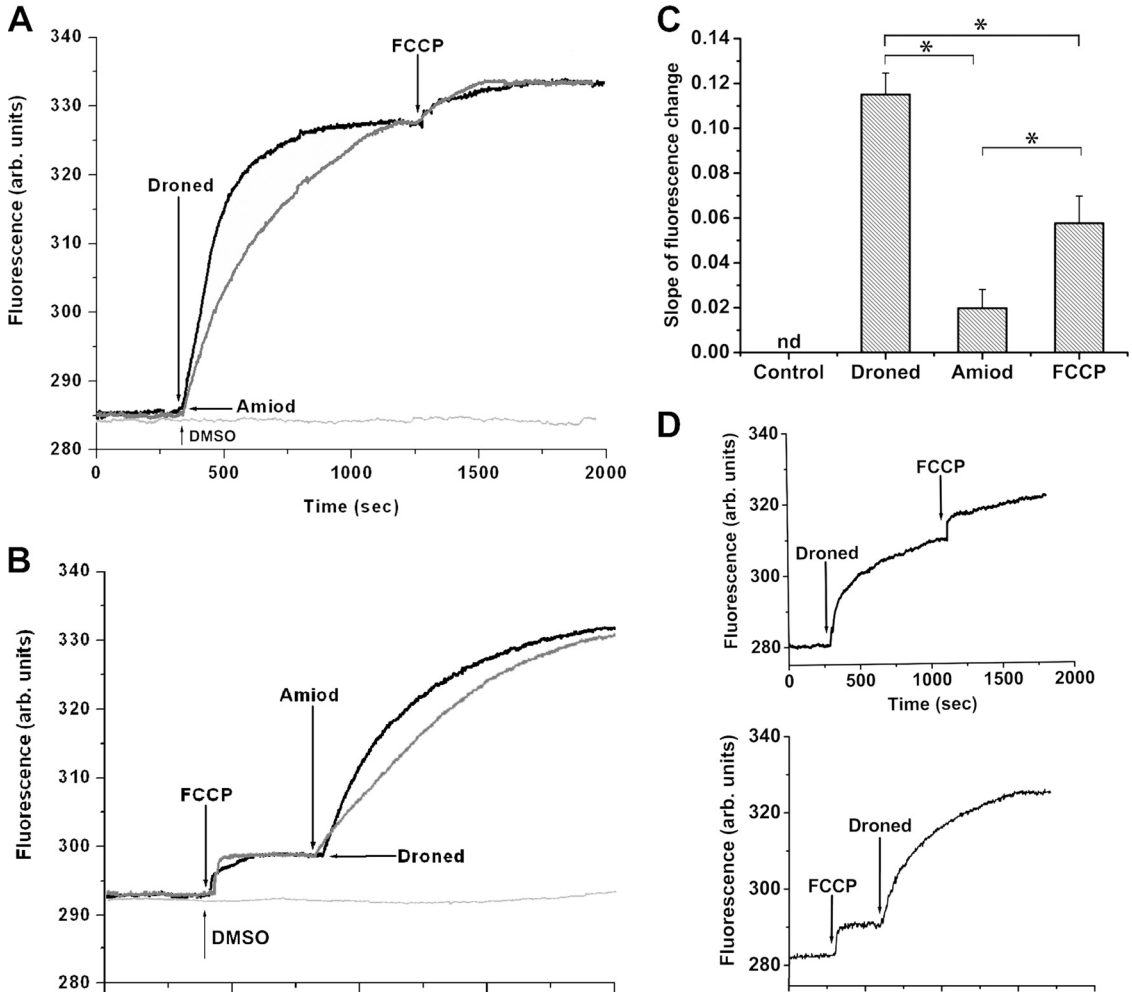

FIG 6 Action of dronedarone on the mitochondrial electrochemical potential of *L. mexicana* promastigotes. Parasites were incubated in the presence of rhodamine 123 for 45 min at room temperature, as indicated under Materials and Methods. (A) Effect of dronedarone (Droned, 2.5 μM), followed by the addition of FCCP (1 μM) on the mitochondrial electrochemical potential (upper black trace). Effect of amiodarone (Amiod, 10 μM) followed by the addition of FCCP (1 μM) on the mitochondrial electrochemical potential (lower gray trace). The additions in panel B are in reverse order versus those in panel A. Arrows indicate the different additions. (C) Initial slopes (300 s) of the curves from experiments similar to those of panels A and B. The slopes corresponding to dronedarone and amiodarone were taken from at least three independent experiments similar to that shown in panel A. The slope corresponding to FCCP was taken from at least three independent experiments similar to that shown in panel B. Each point represents the mean ± SD. *, Significant difference (measured using Student's *t* test, $P < 0.01$). (D) Top, effect of dronedarone (6.5 nM), followed by the addition of FCCP (1 μM) on the release of rhodamine 123 from the mitochondrion; bottom, effects of FCCP (1 μM) and then dronedarone (6.5 nM) on the release of rhodamine 123 from the mitochondrion. The figures are representative of at least three independent experiments.

amiodarone induced a further increase in the release of acridine orange. Once again, the effect of dronedarone was more rapid than that seen with amiodarone (Fig. 5B), perhaps suggesting better cell membrane permeability. Since nigericin completely disrupts acidocalcisome function, this further effect of the drugs suggests that another separate compartment may be involved in their action. Analysis of the initial slopes in Fig. 5A and B indicates (Fig. 5C) that the rate of alkalinization of dronedarone is similar to that obtained with nigericin, while that of amiodarone is significantly slower. This might help explain the lower IC_{50} obtained with dronedarone compared to that with amiodarone (Fig. 5C). We also observed that dronedarone, when added at the IC_{50} (instead of at 2.5 μM), was again able to induce alkalinization of the acidocalcisomes, albeit with a lower velocity (Fig. 5D).

The large, unique mitochondrion in *L. mexicana* is also thought to be involved in $[Ca^{2+}]_i$ regulation (21, 22) and in the leishmanicidal effects of amiodarone (6). Thus, we next investigated the effects of dronedarone on the mitochondrial membrane potential using rhodamine 123, which is known to accumulate in energized mitochondria (4, 9), resulting in self-quenching of the dye's fluorescence. An increase in rhodamine 123 fluorescence corresponds to deenergization. As shown in Fig. 6A, dronedarone (2.5 μM) induces a rapid increase in fluorescence, due to a collapse of the mitochondrial membrane potential. Again, the effect is significantly faster with dronedarone than with amiodarone (at 10 μM) (Fig. 6A). Furthermore, addition of the uncoupler FCCP after addition of either amiodarone or dronedarone induces a small additional release of rhodamine 123, as deduced from the increased fluorescence. When FCCP is added first (Fig. 6B), it induces a rapid but small increase in fluorescence, since FCCP

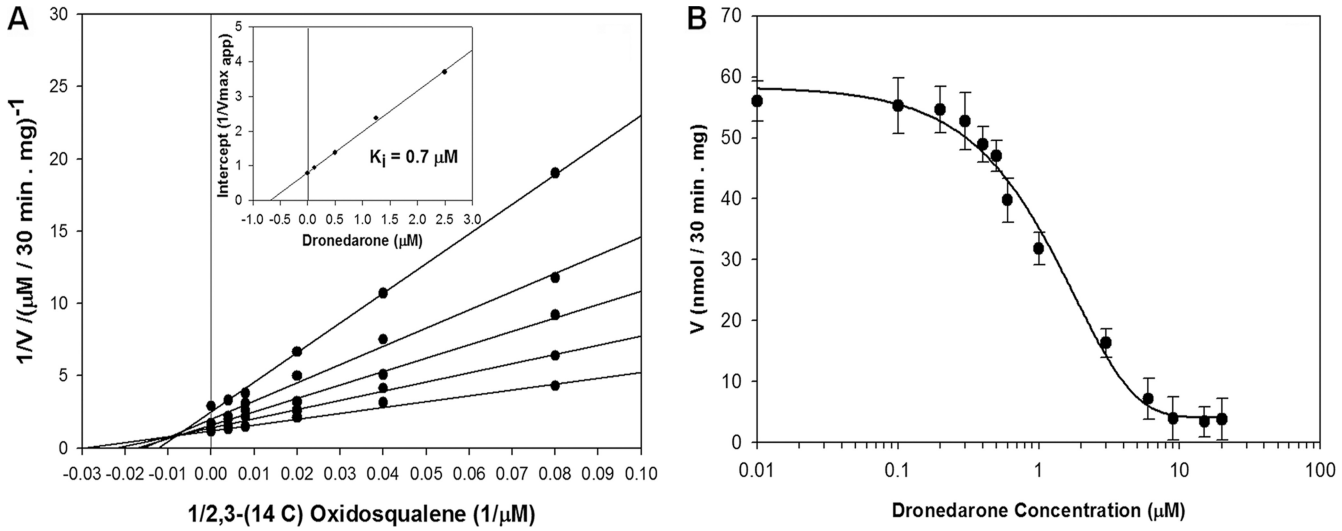

FIG 7 Kinetics and inhibition of *L. mexicana* microsomal OSC. (A) Double-reciprocal plot of LmOSC enzyme activity as a function of the [2,3-^{14}C]oxidosqualene concentration in the presence of the different fixed concentrations of dronedarone. (Inset) Plot of the intercepts as a function of the dronedarone concentration which yields a K_i value of ~0.7 μM. Activity was measured in the presence of 0.1% Triton X-100. (B) Effects of dronedarone on the activity of *L. mexicana* microsomal OSC in the presence of saturating substrate concentrations.

dissipates the mitochondrial membrane potential by permeabilizing the inner mitochondrial membrane to protons. In the same figure, it is also evident that the subsequent addition of dronedarone (2.5 μM) causes a rapid release of rhodamine 123, faster again than that obtained with amiodarone (at 10 μM) (Fig. 6B). The calculated initial slopes of these curves indicate that the effect of dronedarone is faster than that of amiodarone (about 5-fold) and twice as fast as that obtained with FCCP (Fig. 6C). We also performed experiments on the mitochondrial electrochemical potential using the IC_{50} of dronedarone. As can be seen in Fig. 6D, dronedarone is able to induce robust release of rhodamine 123, even when added after FCCP. This strongly suggests that the action of dronedarone on mitochondria might be part of the improved performance of dronedarone compared to that of amiodarone.

From these results, it is clear that dronedarone induces a rapid collapse of the parasite's mitochondrial membrane potential, although its specific target is unknown. The effect of dronedarone or amiodarone after FCCP is not easy to explain since it might be expected that the uncoupler would release all the fluorescent dye. In a previous study with epimastigotes of *T. cruzi* (9), we also observed this behavior with dronedarone (and amiodarone) after FCCP addition. It is conceivable that FCCP is not acting properly under these experimental conditions. Another possible explanation is that part of the action of dronedarone (and amiodarone) occurs by effects on another unknown compartment.

We also performed experiments on the electrochemical mitochondrial potential, using the IC_{50} of dronedarone. It can be seen in Fig. 6D that this drug is also able to induce robust release of rhodamine 123, even when added after FCCP. This strongly suggests that the action of dronedarone on mitochondria may be part of the better performance of dronedarone for these parasites than that of amiodarone.

With amiodarone inhibition of *T. cruzi* growth (6), we reported previously that this drug not only affected the $[Ca^{2+}]_i$ and the mitochondrial membrane potential but also blocked formation of the essential membrane sterol ergosterol by inhibiting the enzyme oxidosqualene cyclase (OSC). We thus investigated whether dronedarone inhibited the activity of *L. mexicana* OSC (LmOSC) in a similar fashion.

Figure 7A shows that the enzyme exhibits classic Michaelis-Menten kinetics with respect to substrates with $K_{m,app}$ [(3*S*)-2,3-oxidosqualene] = 36 μM, $V_{max,app}$ = 0.82 μM · min^{-1}, and V_{max}/K_m = 0.023 min^{-1}. Dronedarone behaves as a potent noncompetitive inhibitor with respect to [(3*S*)-2,3-oxidosqualene], with K_i = 0.7 μM. The dose-response curves for the activity of dronedarone against LmOSC (Fig. 7B) are consistent with noncompetitive inhibition with $K_i \approx IC_{50}$; these K_i values are 1 to 2 orders of magnitude lower than the K_m of the substrates. Similar experiments were performed with amiodarone in order to compare it with dronedarone (not shown). The K_i value obtained was 9.0 μM, much weaker inhibition than that with amiodarone.

To investigate how dronedarone (Fig. 1, compound 2) might bind to LmOSC, we used computational docking with the Glide program (15). The top scoring pose is shown in Fig. 8A and B, superimposed on the structure of the OSC inhibitor Ro-48-8071 (Fig. 1, compound 3) bound to human OSC (PDB code 1W6J). Clearly, it seems very likely that dronedarone binds to the LmOSC substrate binding site with its cationic (trialkylammonium) side chain located close to the essential D718, corresponding to D455 in *Homo sapiens* OSC (HsOSC) that catalyzes the protonation-initiated electrocyclization of epoxysqualene. The binding of amiodarone (Fig. 7C, compound 1) is also similar to that of Ro-48-8071 (Fig. 7C, compound 3) and a comparison between the amiodarone (compound 1) and dronedarone (compound 2) docked LmOSC structures is shown in Fig. 7D. A common feature pharmacophore obtained using the potent known HsOSC inhibitors (Fig. 1, compounds 3 to 7) is shown in Fig. 8E superimposed on the structure of dronedarone (compound 2). The key features of this pharmacophore that are also found in dronedarone are the presence of the cationic feature (that presumably mimics the carbocation obtained on protonation of epoxysqualene) that is likely

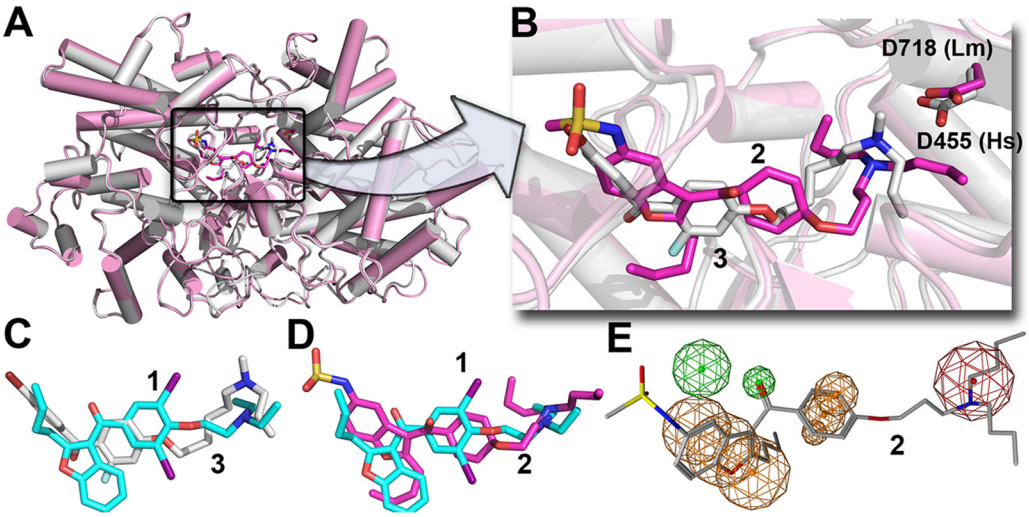

FIG 8 Suggested binding site for dronedarone in *L. mexicana* oxidosqualene cyclase. (A) Glide docking pose of dronedarone (compound 2) bound to a Phyre2-predicted structure model (magenta) superimposed on the X-ray structure of Ro-48-8071 (compound 3, white) bound to human OSC (PDB code 1W6J). (B) Expanded view of panel A, showing the most highly conserved Asp residues in the catalytic site. Dronedarone is in magenta, and Ro-48-8071 (compound 3) is in white. The cationic centers likely interact with the conserved Asp. (C) Superimposed structures of Ro-48-8071 (compound 3) bound to HsOSC and amiodarone (compound 1) docked to the *T. cruzi* OSC model. (D) Comparison between dronedarone (compound 2) and amiodarone (compound 1) docked poses. (E) Common feature pharmacophore for potent HsOSC inhibitors (compounds 3 to 7) superimposed on dronedarone (compound 2) showing common cationic (red) and aromatic/hydrophobic (orange) features.

to interact with the conserved D718, together with 3 hydrophobic features. In conclusion, the results indicate that dronedarone binds to the same catalytic/hydrophobic pocket as does amiodarone (in *T. cruzi* OSC) and the HsOSC inhibitor Ro-48-8071, whose structure is known (PDB code 1W6J) and which has a similar pharmacophore. The results also show that the cationic moiety in dronedarone docks very close to the very highly conserved D718, which in human OSC is a key catalytic residue (D455) involved in the initial squalene epoxide protonation. Given that amastigotes are inhibited with a very low IC_{50} (0.65 nM), it seems unlikely that there will be significant OSC inhibition at the submicromolar levels that might be anticipated to have therapeutic utility. Nevertheless, the development of more potent analogs that target LmOSC is a potentially important goal since multiple-site targeting is expected to increase efficacy.

In conclusion, the results we have shown above are of interest for several reasons. First, we showed that the antiarrhythmia drug dronedarone has activity against *L. mexicana* promastigotes. Second, we showed that it has potent activity against intracellular amastigotes in macrophages, with an IC_{50} of 0.65 nM, while host cell proliferation is not inhibited. These effects are similar to those observed previously with amiodarone but occur more rapidly and are far more pronounced. Third, we found that dronedarone increases intracellular Ca^{2+} and that this increase in $[Ca^{2+}]_i$ arises from Ca^{2+} release from acidocalcisomes and the mitochondrion. Finally, we found that dronedarone inhibits *L. mexicana* oxidosqualene cyclase, potentially opening a future route to block formation of the essential membrane sterol, ergosterol. Overall, these results are of considerable interest since dronedarone is not only more potent than is amiodarone against *L. mexicana* but also known to have fewer adverse side effects (in humans, when used as an antiarrhythmic) because it lacks the iodine substituents that make amiodarone resemble thyroxine or triiodothyronine.

From a clinical perspective, these findings are of importance because mixed infections involving both *Trypanosoma cruzi* and different *Leishmania* species are becoming common clinical scenarios in many countries in Central and South America (23). Thus, having a single drug that can target both parasites is of therapeutic interest. Moreover, *Leishmania mexicana* is a major causative agent of difficult-to-treat diffuse cutaneous leishmaniasis (24), for which new drugs are needed.

It remains to be seen whether dronedarone is more efficacious than is amiodarone in humans since at least part of the efficacy of amiodarone against cutaneous leishmaniasis is likely due to its unusual dermal elimination from the body. That is, concentrations in the skin may be much higher than those with dronedarone, and further work on determining these levels with dronedarone is needed, as are studies aimed at other *Leishmania* parasites. However, the considerably increased efficacy of dronedarone may offset the decrease in skin elimination.

The repositioning of old drugs for their use in other diseases has been a matter of recent interest, since trials in humans have already been successfully conducted, and most of these drugs are not expensive since their patents have expired (25). We postulate that since both dronedarone and amiodarone are inexpensive and amiodarone has been used in some clinical trials against leishmaniasis and also Chagas' disease, both drugs can be repurposed in the near future for the treatment of these human infections. It seems likely that the more potent and less toxic dronedarone may be more efficacious in humans.

Because the role of dronedarone in patients with severe heart failure is still controversial, we believe that its use should be avoided in patients with severe cardiac disease. However, its potential use in otherwise healthy patients with cutaneous leishmaniasis and/or mild to moderate heart failure or arrhythmias remains a feasible therapeutic option, especially considering its potentially high efficacy.

ACKNOWLEDGMENTS

This work was supported by the Fondo Nacional de Ciencia, Tecnología e Investigación, Venezuela (FONACIT) (grant 2011000884), and the Consejo de Desarrollo Científico y Humanístico-Universidad Central de Venezuela (CDCH-UCV) (grant PG-03-8728-2013-1 [to G.B.]) and in part by the NIH (grant GM065307 [to E.O.]).

REFERENCES

1. **Croft SL, Engel J.** 2006. Miltefosine—discovery of the antileishmanial activity of phospholipid derivatives. Trans. R. Soc. Trop. Med. Hyg. **100**(Suppl 1)**:**S4–S8. http://dx.doi.org/10.1016/j.trstmh.2006.03.009.
2. **Croft SL, Olliaro P.** 2011. Leishmaniasis chemotherapy—challenges and opportunities. Clin. Microbiol. Infect. **17:**1478–1483. http://dx.doi.org/10.1111/j.1469-0691.2011.03630.x.
3. **Serrano-Martín X, García-Marchan Y, Fernandez A, Rodriguez N, Rojas H, Visbal G, Benaim G.** 2009. Amiodarone destabilizes the intracellular Ca^{2+} homeostasis and the biosynthesis of sterols in *Leishmania mexicana*. Antimicrob. Agents Chemother. **53:**1403–1410. http://dx.doi.org/10.1128/AAC.01215-08.
4. **Benaim G, Paniz-Mondolfi AE.** 2012. The emerging role of amiodarone and dronedarone in Chagas disease. Nat. Rev. Cardiol. **9:**605–609. http://dx.doi.org/10.1038/nrcardio.2012.108.
5. **Benaim G, Sanders J, Garcia-Marchan Y, Colina C, Lira R, Caldera A, Payares G, Sanoja C, Burgos J, Leon-Rossell A, Concepcion J, Schijman A, Levin M, Oldfield E, Urbina J.** 2006. Amiodarone has intrinsic anti-*Trypanosoma cruzi* activity and acts synergistically with posaconazole. J. Med. Chem. **49:**892–899. http://dx.doi.org/10.1021/jm050691f.
6. **Serrano-Martín X, Payares G, DeLucca M, Martinez JC, Mendoza-León A, Benaim G.** 2009. Amiodarone and miltefosine synergistically induce parasitological cure of mice infected with *Leishmania mexicana*. Antimicrob. Agents Chemother. **53:**5108–5113. http://dx.doi.org/10.1128/AAC.00505-09.
7. **Benaim G, Garcia CR.** 2011. Targeting calcium homeostasis as the therapy of Chagas' disease and leishmaniasis—a review. Trop. Biomed. **28:**471–481.
8. **Benaim G, García-Marchán Y, Reyes C, Uzcanga G, Figarella K.** 2013. Identification of a sphingosine-sensitive Ca^{2+} channel in the plasma membrane of *Leishmania mexicana*. Biochem. Biophys. Res. Commun. **430:**1091–1096. http://dx.doi.org/10.1016/j.bbrc.2012.12.033.
9. **Benaim G, Hernandez-Rodriguez V, Mujica-Gonzalez S, Plaza-Rojas L, Silva ML, Parra-Gimenez N, Garcia-Marchan Y, Paniz-Mondolfi A, Uzcanga G.** 2012. In vitro anti-*Trypanosoma cruzi* activity of dronedarone, a novel amiodarone derivative with an improved safety profile. Antimicrob. Agents Chemother. **56:**3720–3725. http://dx.doi.org/10.1128/AAC.00207-12.
10. **Grynkiewicz G, Poenie M, Tsien RY.** 1985. A new generation of Ca^{2+} indicators with greatly improved fluorescence properties. J. Biol. Chem. **260:**3440–3450.
11. **Concepcion JL, Gonzalez-Pacanowska D, Urbina JA.** 1998. 3-Hydroxy-3-methyl-glutaryl-CoA reductase in *Trypanosoma* (*Schizotrypanum*) *cruzi*: subcellular localization and kinetic properties. Arch. Biochem. Biophys. **352:**114–120. http://dx.doi.org/10.1006/abbi.1998.0577.
12. **Schacterle GR, Pollack RL.** 1973. A simplified method for the quantitative assay of small amounts of protein in biologic material. Anal. Biochem. **51:**654–655. http://dx.doi.org/10.1016/0003-2697(73)90523-X.
13. **Milla P, Viola F, Oliaro Bosso S, Rocco F, Cattel L, Joubert BM, LeClair RJ, Matsuda SPT, Balliano G.** 2002. Subcellular localization of oxidosqualene cyclases from *Arabidopsis thaliana*, *Trypanosoma cruzi*, and *Pneumocystis carinii* expressed in yeast. Lipids **37:**1171–1176. http://dx.doi.org/10.1007/s11745-002-1017-9.
14. **Kelley LA, Sternberg MJ.** 2009. Protein structure prediction on the Web: a case study using the Phyre server. Nat. Protoc. **4:**363–371. http://dx.doi.org/10.1038/nprot.2009.2.
15. **Friesner RA, Banks JL, Murphy RB, Halgren TA, Klicic JJ, Mainz DT, Repasky MP, Knoll EH, Shelley M, Perry JK, Shaw DE, Francis P, Shenkin PS.** 2004. Glide: a new approach for rapid, accurate docking and scoring. 1. Method and assessment of docking accuracy. J. Med. Chem. **47:**1739–1749. http://dx.doi.org/10.1021/jm0306430.
16. **Chemical Computing Group Inc.** 2011. Molecular Operating Environment (MOE). Chemical Computing Group Inc., Montreal, Quebec, Canada.
17. **Schrödinger LLC.** 2010. The PyMOL molecular graphics system, version 1.3r1. Schrödinger, LLC, New York, NY.
18. **Patel C, Yan GX, Kowey PR.** 2009. Dronedarone. Circulation **18:**120:636–644. http://dx.doi.org/10.1161/CIRCULATIONAHA.109.858027.
19. **Docampo R, Scott D, Vercesi A, Moreno SNJ.** 1995. Intracellular Ca^{2+} storage in acidocalcisomes of *Trypanosoma cruzi*. Biochem. J. **310:**1005–1012.
20. **Docampo R, Ulrich P, Moreno SNJ.** 2010. Evolution of acidocalcisomes and their role in polyphosphate storage and osmoregulation in eukaryotic microbes. Philos. Trans. R. Soc. Lond. B Biol. Sci. **365:**775–784. http://dx.doi.org/10.1098/rstb.2009.0179.
21. **Benaim G, Bermudez R, Urbina JA.** 1990. Ca^{2+} transport in isolated mitochondrial vesicles from *Leishmania braziliensis* promastigotes. Mol. Biochem. Parasitol. **39:**61–68. http://dx.doi.org/10.1016/0166-6851(90)90008-A.
22. **Benaim G.** 1996. Intracellular calcium signaling and regulation in *Leishmania*, p 89–106. *In* Tapia R, Caceres-Dittmar G, Sanchez MA (ed), Molecular and immune mechanism in the pathogenesis of cutaneous leishmaniasis. R. G. Landes Co., Medical Intelligence Unit, Austin, TX.
23. **Bastrenta B, Mita N, Buitrago R, Vargas F, Flores M, Machane M, Yacsik N, Torrez M, Le Pont F, Brenière F.** 2003. Human mixed infections of *Leishmania spp*. and *Leishmania-Trypanosoma cruzi* in a sub Andean Bolivian area: identification by polymerase chain reaction/hybridization and isoenzyme. Mem. Inst. Oswaldo Cruz **98:**255–264. http://dx.doi.org/10.1590/S0074-02762003000200015.
24. **Silveira FT, Lainson R, Corbett CE.** 2004. Clinical and immunopathological spectrum of American cutaneous leishmaniasis with special reference to the disease in Amazonian Brazil: a review. Mem. Inst. Oswaldo Cruz **99:**239–251. http://dx.doi.org/10.1590/S0074-02762004000300001.
25. **Novac N.** 2013. Challenges and opportunities of drug repositioning. Trends Pharmacol. Sci. **34:**267–272. http://dx.doi.org/10.1016/j.tips.2013.03.004.